Modeling the Transport of Activated Corrosion Products in the WCLL PbLi Loop for ITER and the EU DEMO With the GETTHEM Code

IEEE Access
Multidisciplinary | Rapid Review | Open Access Journal

Received 6 February 2023, accepted 25 February 2023, date of publication 6 March 2023, date of current version 9 March 2023.

Digital Object Identifier 10.1109/ACCESS.2023.3252905

RESEARCH ARTICLE

Modeling the Transport of Activated Corrosion Products in the WCLL PbLi Loop for ITER and the EU DEMO With the GETTHEM Code

FABRIZIO LISANTI[1], PIETRO ARENA[2], ROBERTO BONIFETTO[1], (Member, IEEE), ANTONIO FROIO[1], FRANCISCO ALBERTO HERNÁNDEZ GONZÁLEZ[3,4], (Member, IEEE), GANDOLFO ALESSANDRO SPAGNUOLO[4], AND ROBERTO ZANINO[1], (Senior Member, IEEE)

[1]NEMO Group, Dipartimento Energia "Galileo Ferraris," Politecnico di Torino, 10129 Turin, Italy
[2]ENEA C. R. Brasimone, 40032 Camugnano (BO), Italy
[3]Institut für Neutronenphysik und Reaktortechnik, Karlsruher Institut für Technologie, 76131 Karlsruhe, Germany
[4]Fusion Technology Department, EUROfusion Consortium, 80331 Garching bei München, Germany

Corresponding author: Antonio Froio (antonio.froio@polito.it)

This work has been carried out within the framework of the EUROfusion Consortium, funded by the European Union via the Euratom Research and Training Programme (Grant Agreement No 101052200 – EUROfusion). Views and opinions expressed are however those of the author(s) only and do not necessarily reflect those of the European Union or the European Commission. Neither the European Union nor the European Commission can be held responsible for them.

ABSTRACT This work presents the results of the implementation in the GEneral Tokamak THErmal-hydraulic Model of available models for the generation and transport of any dispersed material in flowing PbLi eutectic mixture. In particular, the focus is on Activated Corrosion Products circulating as solid suspension in the PbLi loop of the Water-Cooled Lithium-Lead Breeding Blanket of the EU DEMO fusion reactor. A simple test case is used to show that the distribution of the concentration of activated corrosion products at any point of the PbLi loop, both in the water-cooled lithium-lead breeding blanket and in the related ITER Test Blanket System, can be determined by the model. Moreover, thanks to the model's dynamic nature, operational transients can be simulated; for instance, starting from zero impurities in the PbLi alloy, the evolution of the concentration of corrosion products is shown, until the steady-state is reached. The results obtained with this tool can be useful not only for radiological safety purposes, but also because activated corrosion products may affect the PbLi flow itself and the efficiency of the tritium removal system, with consequences on the achievable Tritium Breeding Ratio. A rigorous verification of the model is also performed.

INDEX TERMS Activated corrosion products, blanket, ITER, modelling, nuclear fusion.

I. INTRODUCTION

The design of the EU DEMO, performed by the EUROfusion Consortium [1], takes advantage of different computational tools, often aimed at modelling single physics and/or single systems. However, system-level tools used for plant integration studies require different pieces of physics and/or different subsystems to be modelled at the same time; this is one of the aims of the system-level GEneral Tokamak THErmal-hydraulic Model (GETTHEM), developed at Politecnico di Torino since 2015 [2], for the thermal-hydraulic modelling of the Breeding Blanket (BB) and related subsystems, e.g. the Primary Heat Transfer System (PHTS) and the Balance-of-Plant. The code was applied in the past for the thermal-hydraulic transient analysis of the Helium-Cooled Pebble Bed and Water-Cooled Lithium-Lead (WCLL) [3] BB designs in normal and off-normal scenarios [4], [5]. In recent years, a model of the WCLL PbLi loop was introduced in GETTHEM, including MHD pressure drops [6], but a comprehensive model of the PbLi loop must include also additional models relevant to plant operation and safety – e.g. for tritium production, transport, and extraction, as well as for the transport of other radioactive elements such as the Activated Corrosion Products (ACPs) – since the different phenomena involved are interdependent with each other, hence a self-consistent model should be able to address them

The associate editor coordinating the review of this manuscript and approving it for publication was Claudia Raibulet.

at the same time. The need for a self-consistent assessment of this phenomenon with a multiphysics approach is also highlighted by the recent efforts to couple the OSCAR tool for the assessment of the ACPs with other codes such as MCNP [7] or RAVEN [8], which are being pursued for the water cooling loops of the PHTS of tokamaks, but is still missing for liquid metal systems [9].

This work presents the implementation in GETTHEM of a model for the assessment of the generation and transport of ACPs in the WCLL PbLi loop. Taking advantage of the object-oriented nature of the GETTHEM code (and of its underlying modelling language, Modelica), the model is integrated in the existing WCLL package of the GETTHEM code and applied to the EU DEMO WCLL BB PbLi loop, as well as to that of the ITER WCLL-Test Blanket System (TBS), which is one of the TBS proposed by Fusion for Energy (F4E), the EU domestic agency for ITER, for inclusion in the Initial Configuration (InCo) of the ITER Test Blanket Module (TBM) program. Thanks to this new system-level model, it is possible to determine the quantity and the location of the corrosion products within the PbLi circuit during both normal and off-normal scenarios; if data concerning the specific activity of the corroded species are available, an estimation of the radioactive inventories in different locations of the circuit can then be carried out, supporting the definition of the appropriate radiation barriers.

The issue of the generation of corrosion products in liquid-breeder loops has already been addressed in the past from an experimental point of view, for instance in [10] with reference to the development of a liquid breeder TBM (using either liquid lithium or PbLi) for the Korean DEMO, but with no focus on the modelling of this phenomenon at the system level. Conversely, other system-level tools for the dynamic simulation of liquid metal or molten salt BB loops already exist, e.g. a code developed with the EcosimPro simulation platform including the tritium transport modelling in the PbLi loop of the HCLL-TBS [11], or a thermal-hydraulic model of the FLiBe loop of the ARC reactor developed with Modelica [12], or models to predict MHD pressure drops in PbLi implemented in the system-level thermal-hydraulic code RELAP5/MOD3.3 [13]. However, to the best of the authors' knowledge, a system-level analysis on the generation and transport of ACPs in the WCLL PbLi loop was yet to be performed.

II. DESCRIPTION OF THE MODEL

The GETTHEM code is written using the Modelica language, and it is based on the Modelica Standard Library (MSL) and on the (validated) ThermoPower library [14]. The code is based on a modular approach, allowing simple modelling of complex systems with a graphical interface, and enabling the generation of new models by extending existing objects, thanks to the object-oriented approach.

A. MODEL ASSUMPTIONS

The model provides the possibility to include the transport of an unlimited number of dispersed materials (DMs) within the working fluid: in this work only ACPs are considered, but its application to the transport of other DMs is straightforward. As a matter of fact, different models for the generation and removal of tritium and helium will be implemented to extend the application of the model also to the transport of such DM species, and the results have been presented elsewhere [15]. Note that the transport of DM particles within the fluid is modelled in this work as a scalar transport.

The core assumption behind the model is that the DM particles are found in the fluid in trace concentration only, meaning that they do not affect the thermophysical properties of PbLi. Both the MSL and ThermoPower libraries, on which the GETTHEM code is based, expose an interface to model the transport of trace substances in a fluid stream, according to the Modelica.Media definition [16], [17], under the assumption that their presence does not significantly affect the fluid properties. The model described in this work is based on this interface and is thus fully compatible with other Modelica.Media-compliant libraries, such as the GETTHEM code.

In view of the low fluid velocity, the PbLi flow is assumed to be incompressible. Moreover, it is assumed for this work that MHD does not affect the transport of DMs, since no information or experimental data are available on the subject. The mass balance for each DM is solved, assuming two distributed source terms and one distributed sink term, namely:

- S_C : corrosion of activated material (in-box corrosion, source term).
- S_A : activation of corroded material (source term).
- S_R : redeposition of corroded material (sink term).

These three terms are implemented but not modelled in detail within the code: they must be provided in input as external functions to the components featuring these terms.

Concerning the removal of the ACPs from the PbLi loop, one option is to use Cold Traps (CTs), which will not manage to remove ACPs from the PbLi when their concentration is above saturation [18]. For this reason, the CT is modelled with a constant removal efficiency and assumed to operate when the concentration of each ACP species is larger than its respective saturation limit.

B. MODEL IMPLEMENTATION

Most of the models already implemented in GETTHEM are based on components available in the free and open source ThermoPower library; however, ThermoPower models are optimized for modelling compressible gas or water flows, while in this model, as mentioned in section II-A above, the PbLi flow is assumed to be incompressible. Therefore, the new components rely on the Modelica.Fluid package available in the MSL [17], which is also a free and open-source library. Note that, thanks to the object-oriented nature of the code, this does not introduce compatibility issues with

existing GETTHEM models, as all of them are based on the same interfaces.

Two new components have been added to the GETTHEM library: a model for the 1D flow in a pipe or duct, including the three source/sink terms discussed in section II-A above, to be used for the components where corrosion and/or activation takes place, and a 0D model for the CT. In the 1D flow model, in addition to the mass, momentum, and energy conservation equations for the fluid, the mass conservation for the generic j-th DM species is solved,

$$A\left(\frac{\partial \rho_{DM,j}}{\partial t}+\frac{\partial\left(\rho_{DM,j} v\right)}{\partial x}\right) = s_{C,j}(x,t)+s_{A,j}(x,t)-s_{R,j}(x,t) \quad \forall j \in [1,N_S] \tag{1}$$

where N_S is the number of different species, A is the cross section of the pipe/duct, $\rho_{DM,j}$ is the density of the j-th DM species, t is time, v is the speed of the working fluid, x is the coordinate representing the 1D flow direction, and $s_{C,j}$, $s_{A,j}$ and $s_{R,j}$ (in kg/(m·s)) are the linear corrosion and activation sources, and redeposition sink, respectively, for the j-th DM species. Due to the assumption of an incompressible flow, the continuity equation for the working fluid in 1D becomes $\frac{\partial v}{\partial x}=0$, so that v can be taken out of the space derivative terms, and (1) becomes

$$A\left(\frac{\partial \rho_{DM,j}}{\partial t}+v\frac{\partial \rho_{DM,j}}{\partial x}\right) = s_{C,j}(x,t)+s_{A,j}(x,t)-s_{R,j}(x,t) \quad \forall j \in [1,N_S] \tag{2}$$

The space derivative is approximated using the Finite Volume (FV) approach with an upwind scheme, i.e. splitting the domain in N_V control volumes (CV) of equal length Δx and centroid x_i, and integrating (1) in space over each CV,

$$\frac{dM_{DM_j,i}}{dt} = \dot{m}_{DM_j,i,in}(t)+\dot{m}_{DM_j,i,out}(t)+S_{C,i,j}(t)+S_{A,i,j}(t) - S_{R,i,j}(t) \; \forall j \in [1,N_S], \quad \forall i \in [1,N_V], \tag{3}$$

where $M_{DM_j,i}$ is the mass of the j-th DM species in the i-th CV, $\dot{m}_{DM_j,i,in/out}$ is the mass flow rate of the j-th DM species entering the i-th CV at its inlet/outlet (i.e. negative if exiting), and $S_{C,i,j}(t)=s_{C,j}(x_i,t)\,\Delta x$, $S_{A,i,j}(t)=s_{A,j}(x_i,t)\,\Delta x$, and $S_{R,i,j}(t)=s_{R,j}(x_i,t)\,\Delta x$ (in kg/s) are the local corrosion and activation sources, and redeposition sink, respectively, for the j-th DM species, in the i-th CV (i.e. the midpoint quadrature formula is used). The value for $\dot{m}_{DM_j,i,in/out}$ is chosen at the upstream boundary (i.e., the one where the fluid is entering the CV) automatically according to the flow direction, as per the upwind scheme.

For consistency with the Modelica.Media description for trace substances, the equation is rewritten in terms of dimensionless mass concentration $C_j = M_{DM_j}/M$, where M is the mass of the working fluid, as

$$M_i\frac{dC_{i,j}}{dt} = \dot{m}_{i,in}(t)\,C_{i,j,in}(t)+\dot{m}_{i,out}(t)\,C_{i,j,out}(t)+S_{C,i,j}(t) + S_{A,i,j}(t)-S_{R,i,j}(t) \; \forall j \in [1,N_S], \quad \forall i \in [1,N_V], \tag{4}$$

where $\dot{m}_{i,in/out}$ is the working fluid mass flow rate entering the i-th CV at its inlet/outlet (i.e. negative if exiting), $C_{i,j}$ is the concentration of the j-th DM species in the i-th CV, and $C_{i,j,in/out}$ is the upstream concentration of the j-th DM species at the i-th CV boundary (inlet/outlet), chosen according to flow direction. The $3\times N_S$ terms $S_{C,j}$, $S_{A,j}$, and $S_{R,j}$ must be provided as inputs, as a function of the local coordinate x. To avoid numerical issues arising due to the possibly very small values of C_j (when expressed in kg_{DM}/kg_{PbLi}), the equation is internally rewritten in terms of $\hat{C}_j = C_j/C_{j,nom}$, where $C_{j,nom}$ is a nominal value of the concentration for the j-th DM, to be provided as input.

The time derivative of the ACPs concentrations in (4) is not neglected in order to make the model as generic as possible, making it applicable to different test cases or different scenarios (e.g. accidental transients) where the timescale of accumulation of ACPs inside the component becomes non-negligible compared to the timescales relevant to the PbLi circuit. Considering the PbLi loop of the EU DEMO WCLL, for instance, the flow velocity inside the BB is so small that the PbLi transit time inside it represents a major part of the overall transit time inside the whole circuit (see section IV-E).

Concerning the CT model, in addition to a 0D mass and energy balance, it computes the concentration at the outlet as a function of the concentration at the inlet:

$$C_{j,out} = f\left(C_{j,in}\right) \quad \forall j \in [1,N_S]. \tag{5}$$

According to [18], the following constant efficiency equation (6) is applied by default only when $C_{j,in}$ is larger than the saturation concentration for the j-th DM species C_j^S

$$f\left(C_{j,in}\right) = \begin{cases} C_{j,in} & \text{for } C_{j,in} \le C_j^S \\ C_j^S + (1-\eta_j)\left(C_{j,in}-C_j^S\right) & \text{for } C_{j,in} > C_j^S \end{cases} \quad \forall j \in [1,N_S], \tag{6}$$

where η_j is the cold trap efficiency associated to the j-th DM, to be provided in input as a fixed parameter.

III. VERIFICATION

The verification of the new 1D model implementing the mass balance equation for DM species, introduced in section II, has been performed to assess its reliability and accuracy. Given that equivalent numerical tools, as explained in section I, were not available yet, a benchmark could not be performed; therefore, the Order-of-Accuracy (OoA) test has been carried out for the model verification, adopting the method of the manufactured solution (MMS).

The MMS [19] is used to verify the correct implementation of the discretization procedure for a set of Partial Differential Equations (PDEs). The concept behind this method is to choose an arbitrary (''manufactured'') solution and substitute it in the original PDE – or system of PDEs – in order to generate fictitious source terms to be implemented in the discretized set of PDEs. At this point the convergence of

the numerical solution to the manufactured one is studied, varying the mesh size used for the discretization, to determine whether the discretization error changes at the expected rate.

In this work, the MMS has been applied to the mass balance equation for DM species, presented in (1), bearing in mind that the density of the j-th DM species can be written in terms of its concentration C_j in PbLi as

$$\rho_{DM,j} = \rho_f C_j \quad \forall j \in [1, N_S], \tag{7}$$

where ρ_f is the working fluid density. The following manufactured solution was chosen for the concentration C_j of a generic DM species

$$C_j = B\left[1 + \sin\left(\frac{\pi x}{L}\right)\right]\left[1 - \exp\left(-\frac{t}{t_0}\right)\right], \tag{8}$$

where $B = 10$ and $t_0 = 30$ s are constants, L is the pipe length, t is the time variable, and x is the space coordinate along the flow path within the pipe. A fictitious source term Q_j is introduced in the continuity equation

$$\rho_f \frac{\partial C_j}{\partial t} + \rho_f \frac{\partial \left(C_j v\right)}{\partial x} = Q_j, \tag{9}$$

Imposing the manufactured solution for C_j in the DM mass balance equation, the fictitious source term Q_j is found

$$\begin{aligned} Q_j = &\frac{\rho_f B}{t_0}\left[1 + \sin\left(\frac{\pi x}{L}\right)\right]\exp\left(-\frac{t}{t_0}\right) \\ &+ \frac{\rho v B \pi}{L}\left[1 - \exp\left(-\frac{t}{t_0}\right)\right]\cos\left(\frac{\pi x}{L}\right), \end{aligned} \tag{10}$$

which is implemented in the discretized continuity equation of the model

$$\begin{aligned} M_i \frac{dC_{i,j}}{dt} = &\dot{m}_{i,in}\left(t\right) C_{i,j,in}\left(t\right) + \dot{m}_{i,out}\left(t\right) C_{i,j,out}\left(t\right) \\ &+ Q_{i,j}\Delta x A \quad \forall j \in [1, N_S], \ \forall i \in [1, N_V], \end{aligned} \tag{11}$$

where $Q_{i,j}$, evaluated in each CV, is multiplied by the volume $\Delta x A$ of the i-th CV to convert it to kg/s.

The convergence study was performed on a trivial test case where the pipe model implementing the DM balance equation is placed between a mass flow source and a sink. A length $L = 0.862$ m and hydraulic diameter $D_h = 0.122$ m for the pipe model, and a temperature $T = 330$ °C and mass flow rate $\dot{m} = 1$ kg/s for the PbLi flow were adopted. Fig. 1 shows the results of the verification and convergence analysis. The relative error on the computed solution C_j (shown in Fig. 1b) halves when the Δx is halved, resulting in an OoA of the 1st order, as expected considering the FV approximation with an upwind scheme [20].

It must be noted that the computed discretization error is specific to the case study adopted for the verification – and it cannot be considered a priori correct for other test cases – since it depends on the set of input parameters and flow operating conditions assumed for each test case. However, the verification study performed in this work was meant, in the first place, as a check of the correct implementation of the model equations (i.e. if the order of convergence was the expected one, given the discretization method used), and it allowed to have a qualitative estimation of the accuracy of the solution related to the spatial discretization.

The verification and convergence study reported above has been carried out for the space discretization only; indeed, for the time marching scheme, the DASSL solver [21], available in the Dymola and OpenModelica compilers and already verified, has been used, which is a variable-order, variable-step solver, thus not allowing a direct control of the time-step.

IV. TEST CASES

To test the model, two test cases for the PbLi loop have been developed, including a detailed model only for the set of components strictly necessary for the analysis of the ACPs transport and removal, based on the ITER WCLL-TBS PbLi loop (hereafter referred to as test case I) and on the PbLi loops for EU DEMO (hereafter referred to as test case II); for instance, the model does not include the tritium permeation phenomena in the Tritium Extraction and Removal (TER) system at this stage. Nevertheless, the main aim of this test case is to showcase the capability of the code to compute the ACP distribution along the PbLi loop, and not to provide final results.

A. TEST CASE I: THE ITER WCLL-TBS PBLI LOOP

The PbLi loop [22], [23], [24] is one of the ancillary systems of the ITER WCLL-TBS, consisting of a closed circuit where forced circulation of the PbLi eutectic alloy is provided to ensure and maintain suitable operating conditions for the TBM regular operation. Other important functions of this system are: (i) to allow the extraction of the tritium produced inside the WCLL-TBM box, (ii) to remove impurities (such as ACPs) from the PbLi alloy, and (iii) to allow the confinement of radioactive products.

Besides the TBM box, the PbLi loop is made of several sub-systems, shown in Fig. 2; the main ones are:

- the TER system.
- the Heater (HT).
- the Cooler (HX).
- the CT.
- the Storage/Recirculation Tank (ST).
- the Pump (PL1).

In normal operating conditions, the PbLi flow exits the TBM box at a temperature of 330 °C; at this point it passes through the HT, where it is heated up to 450 °C to improve the extraction efficiency, before entering the TER where the tritium solubilized in the PbLi alloy is extracted. The PbLi flow is then cooled down to 300 °C by the HX and split in two branches: a first portion of the flow enters the CT, where impurities are removed from the alloy, before being merged with the remaining part of the flow and sent to the ST, where an inert Helium atmosphere is present to avoid the oxidation of the lithium. Finally, the PbLi is pumped from the tank by the Circulation Pump and directly routed back to the WCLL-TBM.

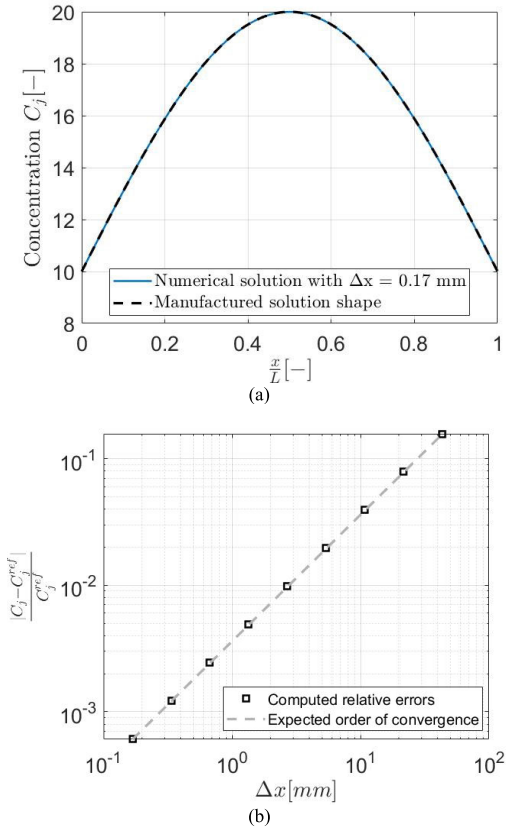

FIGURE 1. Results of the verification and convergence analysis: (a) shape of the numerical solution (solid line) computed imposing the fictitious source term, compared to the manufactured solution (dashed line), and (b) convergence analysis for the concentration C_j where the expected order of accuracy is depicted with the gray dashed line.

The ITER WCLL-TBM, described in detail in [25], is a box made of a vertical C-shaped First Wall (FW) closed on the sides by Side Caps and on the back by four Back Plates (BPs), acting as manifolds for the coolant and breeder flow distribution. A set of poloidal-radial and toroidal-radial stiffening plates splits the box volume into 16 internal cells, called Breeding Units (BUs), where PbLi is circulating at low speed. A global view of the ITER WCLL-TBM is shown in Fig. 3. The PbLi entering the TBM is collected in the manifold and distributed to the BUs, each of which is divided in two halves in the poloidal direction by means of a Baffle Plate. Hence, the PbLi enters the lowest BU half from the manifold, and it radially travels towards the FW; it then makes an upward U-turn around the baffle plate into the top half of the BU, exiting the cell from the BPs.

B. TEST CASE II: THE EU DEMO WCLL PBLI LOOPS

The WCLL concept for the EU DEMO BB has several separate PbLi circuits for the inboard (IB) and the outboard (OB) BB regions, because the PbLi is supplied to the entire blanket, not only to a single TBM, as for the case of the ITER TBS. The current DEMO reference configuration foresees 16 sectors for the BB, each of which consists of five BB segments: three in the OB region – left, central and right OB segments (LOB, COB and ROB, respectively) – and two for the IB region – left and right IB segments (LIB and RIB, respectively). The BB sectors are fed by four PbLi loops for the OB segments (12 OB segments fed by each loop) and two PbLi loops for the IB segments (16 IB segments fed by each loop) [3], [26].

The PbLi coming from the main equipment region (where TER system, heat-exchangers, circulation tanks and other components are placed) is sent by the pump to the lower ring manifold, from where it enters the BB segments from the bottom through the inlet legs. Here the fluid flows inside the inlet manifold and it is distributed to the breeding zone (BZ); the latter, analogously to the WCLL-TBS, is split by toroidal-radial stiffening plates (see Fig. 4) in a set of BUs (stacked on top of each other in the poloidal direction) where PbLi flows in the radial direction with a U-shaped path around a baffle plate before entering the outlet manifold. Poloidal-radial stiffening plates separate the BUs in a set of rectangular cross-section channels. The fluid exits the BB segments from the top through the outlet legs, is collected by the upper ring manifold and is sent back to the main equipment region. Fig. 5 shows a view of the EU DEMO WCLL PbLi loop.

C. CASES DESCRIPTION

The linear corrosion source term s_C can be computed as

$$s_C(x,t) = \omega \rho_W \chi(x,t), \tag{12}$$

where ω is the wetted perimeter, ρ_W is the density of the wall (assumed constant), and χ is the corrosion rate (in m/s). For the purposes of this test, the Sannier correlation [28] has been implemented to compute the corrosion rate as

$$\chi(x,t) = 2.535 \cdot 10^{-4} \exp\left(-\frac{25690}{1.98T(x,t)}\right) v(x,t)^{0.875} D_h^{-0.125}, \tag{13}$$

where T and v are the temperature (in K) and speed (in m/s) of the working fluid, respectively, and D_h is the hydraulic diameter of the pipe/duct. It should be noted that the validity of the Sannier correlation, at the low speed typical of the PbLi flow in the WCLL BB and TBS, is still to be verified; nevertheless, it was shown in [29] to agree to a reasonable accuracy with experimental data, hence it is used here in the absence of better information. In addition, the Sannier correlation was already used in the past for WCLL-TBS-relevant analyses [18].

In order to have a comprehensive view of the generation and removal of ACPs inside the PbLi loop, the non-radioactive corrosion products generated in the loop, and then activated while exposed to the neutron flux in the TBM box, should also be assessed. For the sake of testing the model in the present work, this contribution (source term S_A) has been set equal to zero, due to the lack of an activation model. The same is true for the redeposition sink term S_R, which would require a detailed chemical modelling. The reason behind these assumptions is due to missing information

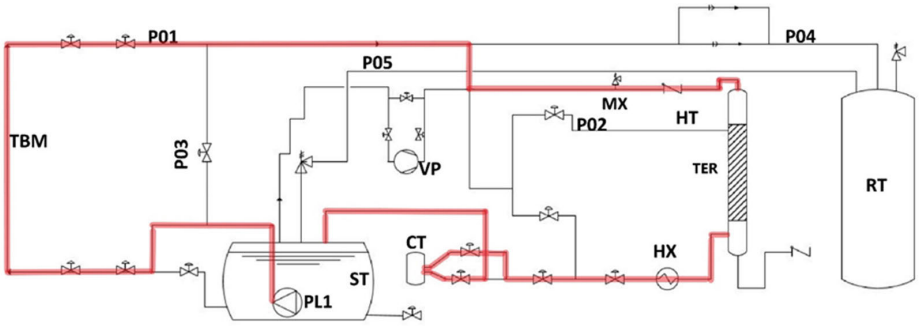

FIGURE 2. Simplified scheme of WCLL-TBM PbLi loop: the loop modelled in this work is highlighted in red. P01-05 are pipelines. Other components not modelled here are the mixer (MX), the relief tank (RT) and the vacuum pump (VP). (Adapted from [24]) .

about these terms in literature, to the best of the authors' knowledge. However, both contributions could be provided to the code as external functions once a characterization of these phenomena is available.

The model for test case I, shown in Fig. 6, features the main components of the WCLL-TBS PbLi loop listed in section IV-A; lead-lithium pipes (distribution pipes, external pipes etc.) are also included.

The TBM and CT models are described in section II-B, whereas all the other objects are available within the MSL.

The TBM model is split into two objects, *TBM_in* and *TBM_out* in Fig. 6, representing the bottom and top half of the BU, respectively. The PbLi flow U-turn around the baffle plate, from the bottom to the top BU half, is modelled by means of the *CurvedBend* object – available within the MSL – as a localized pressure drop $\Delta p_{loc} = k\rho v^2/2$, where k is the localized friction factor and ρ is the working fluid density. Moreover, to be compliant with the WCLL-TBS operating conditions presented in section IV-A, the PbLi is assumed to increase its temperature from 300 °C to 330 °C uniformly along the TBM.

The model for the TBS Pbli loop includes distribution pipes, external pipes, loop pipes and the so-called Pipe Forest, a network of pipes that connects the Ancillary Equipment Unit (which includes the PbLi system) to the TBM at the equatorial port-plug level [30]. MSL pipe objects are used to model these components, consisting in simple 1D flow models implementing the mass, momentum and energy balance equations. Moreover, for the centrifugal pump model included in the circuit, the characteristic curve is reported in Table 1. The HT and the HX, placed upstream and downstream the TER system, respectively, are modelled as ideal heat exchangers. Therefore, the temperature at the outlet of the two heat exchangers will always be equal to that on the secondary side, that is 450 °C for the HT and 300 °C for the HX.

For the test case II, two PbLi loop models have been built, one for a IB loop and one for a OB loop, shown in Fig. 7. The two IB and OB loops feature the same set of objects: the components of the main equipment region (i.e. 2 heat exchangers, TER system, CT, circulation tank and PbLi pump), the loop pipes (upper/lower ring manifolds, inlet/outlet legs) and the BB segments. IB and OB loop models differ in PbLi mass flow rates, dimensions and number of pipes. The PbLi storage tank (see Fig. 5), collecting all the plant PbLi when the 6 loops are drained, is not modelled in this work, since it is excluded during operation.

The BB objects are modelled by three 1D pipe objects implementing the corrosion term (described in section II-B) connected in series, representing the inlet manifolds, BUs and outlet manifolds, respectively (for a detailed view see Fig. 7a). For the sake of simplicity, the dimensions of the BUs are assumed uniform along each segment and equal to the ones of the BU on the equatorial plane. Three different (in geometry) BB objects are modelled: one for the IB segments (LIB and RIB segments are identical, hence modelled by the same object) and two for the COB and the L/ROB segments (again, LOB and ROB are identical), each of them modelling all the corresponding segments fed by the loop. In the OB loop model, the L/ROB and COB BB objects are connected in parallel.

In test case II, corrosion of EUROFER97 is assumed to take place in the PbLi loop pipes too, hence they are modelled with the model presented in this work.

The model for the CT in test case II is the one described in section II-B (as for test case I), while the two heat exchangers (HX1 and HX2), placed upstream and downstream the TER system, are both modelled as ideal heat exchangers with the same secondary side temperature of 330 °C.

Since the models for the 2 test cases are limited to the analysis of the generation and transport of ACPs only, the TER object used for this work in both test cases does not model the phenomena involved in the tritium extraction, but, at this stage, it consists of a simple 1D pipe model implementing the mass, momentum and energy balance equations for the PbLi flow.

The PbLi is assumed to uniformly corrode the EUROFER97 surfaces; For the time being, only Fe and Cr are considered, as they are expected to be the most important contributors to the total ACP activity, whereas the corrosion of other materials, such as Ni or Mn, is assumed negligible [18]. The mass source term is therefore split between Fe and Cr

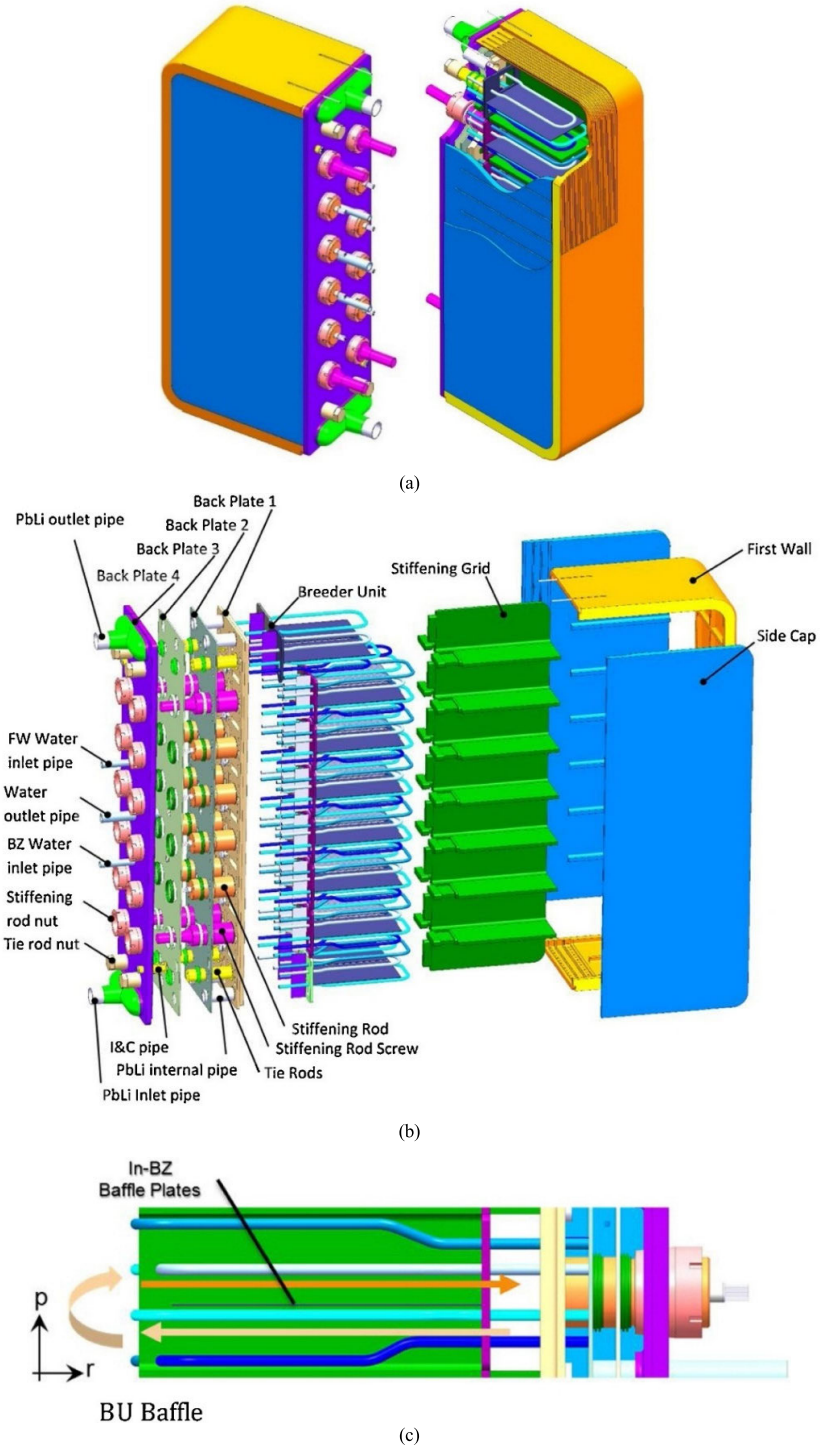

FIGURE 3. ITER WCLL-TBM box: (a) global view and (b) exploded view of the TBM, and (c) poloidal-radial cut of the BU showing the PbLi circulation (adapted from [25]).

according to their nominal concentration (i.e., 89% and 8.9%, respectively):

$$s_{C,Fe} = 0.89 s_C; \tag{14}$$

$$s_{C,Cr} = 0.089 s_C. \tag{15}$$

Considering the CT, the calculation of C_j^S in (6) is performed by the model for Fe and Cr according to [18]

$$C_{Fe}^S = 10^{-6} exp\left(13.604 - \frac{12975}{T}\right), \tag{16}$$

$$C_{Cr}^S = 4.92 \cdot 10^{-8} exp\left(0.0058T\right), \tag{17}$$

where T is the local temperature (in K) of the working fluid and C^S is expressed in kg_{DM}/kg_{PbLi}.

TABLE 1. Input parameters for test case I.

TBM		
Number of BU channels	16	-
Number of CVs	5120	-
Channel length	0.862	m
Channel hydraulic diameter	0.122	m
Wall density	7798	kg/m^3
COLD TRAP		
Pipe length	0.4	m
Pipe diameter	0.122	m
ACP removal efficiency	0.9	-
PUMP		
Nominal rotational speed	1200	r.p.m.
Nominal fluid density	9806	kg/m^3
Nominal head	1.2	bar
Flow characteristic:	$H = -1.6514 \times 10^6 Q^2 - 254.8420Q + 2.6655$ H: head (in m) Q: volumetric flow rate (in m^3/s)	
HEATER		
Secondary side temperature	723.15	K
Pipe length	0.5	m
Pipe diameter	0.122	m
COOLER		
Secondary side temperature	573.15	K
Pipe length	0.5	m
Pipe diameter	0.122	M
TER		
Pipe length	1.9	m
Pipe diameter	0.04	m
STORAGE/RECIRCULATION TANK		
Height	10	m
Initial level	5	m
Surface pressure	4.2	bar
Cross sectional area	1	m^2
PbLi FLOW		
Nominal mass flow rate	1	kg/s
Nominal pressure	10	bar
Nominal temperature range	573.15 – 723.15	K
Total pressure drop	1	bar
LOOP PIPES		
Total length	18.4	m
Internal diameter	26	Mm
PIPE FOREST		
Total length	30.3	m
Internal diameter	41	Mm
PbLi EXTERNAL PIPES		
Total length	3.197	m
Internal diameter	45	mm
PbLi DISTRIBUTION PIPES		
Total length	40.15	mm
Internal diameter	65	mm

The geometrical data used for the PbLi loop pipes, and all the other inputs required to run the model are reported in Table 1 for test case I and in Table 2 for test case II.

TABLE 2. Input parameters for test case II.

	IB LOOP	OB LOOP	
BB			
Number of segments per loop	16	8 (LOB+ROB) 4 (COB)	-
Number of BUs per segment	92	104 (COB) 103 (L/ROB)	-
BU channel length	0.358	0.548 (COB) 0.539 (L/ROB)	m
BU channel hydraulic diameter	0.088	0.098 (COB) 0.100 (LOB)	m
Inlet/Outlet manifold length	12.565	14.154 (COB) 13.989 (LOB)	m
COLD TRAP			
Pipe length	0.4	0.4	m
Pipe diameter	0.250	0.250	m
ACP removal efficiency	0.9	0.9	-
PUMP			
Nominal rotational speed	1200	1200	r.p.m.
Nominal fluid density	9802.6	9802.6	kg/m^3
Nominal head	1.2	1.2	bar
Flow characteristic: (H: head [m], Q: vol. flow rate [m^3/s])	$H = -262.3\ Q^2 - 2.2616\ Q + 1.3215$	$H = -335.0\ Q^2 - 2.5556\ Q + 1.3215$	
HEAT EXCHANGERS			
Secondary side temperature	603.15	603.15	K
Pipe length	0.5	0.5	m
Pipe diameter	0.250	0.250	m
TER			
Pipe length	40	40	m
Pipe diameter	0.3	0.3	m
CIRCULATION TANK			
Height	10	10	m
Initial level	5	5	m
Surface pressure	41.2	41.2	bar
Cross sectional area	1	1	m^2
PbLi FLOW			
Nominal mass flow rate	249.3	281.7	kg/s
Nominal pressure	46	46	bar
Nominal temperature	603.15	603.15	K
LOWER RING MANIFOLD			
Pipe length	65	50	m
Pipe internal diameter	258.8	258.8	mm
Number of pipes per loop	1	1	-
UPPER RING MANIFOLD			
Pipe length	65	50	m
Pipe internal diameter	258.8	258.8	mm
Number of pipes per loop	1	1	-
INLET LEG			
Pipe length	27	25	m
Pipe internal diameter	133.3	208.3	mm
Number of pipes per sector	2	3	-
OUTLET LEG			
Pipe length	3	6.1	m
Pipe internal diameter	160.3	208.3	mm
Number of pipes per sector	2	3	-
OUTLET LEG – IN PORT MANIFOLD			
Pipe length	17.5	9.7	m
Pipe internal diameter	160.3	258.8	mm
Number of pipes per sector	1	1	-

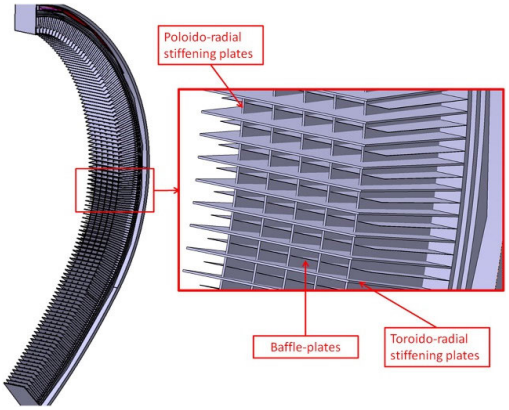

FIGURE 4. WCLL BB segment view; detail of the BZ internal structure [27].

D. RESULTS: TEST CASE I

The model is run to simulate a transient of four days, starting from a DM concentration in PbLi equal to zero and assuming a constant pump speed. The evolution of the Fe and Cr concentration at the outlet of the CT is reported in Fig. 8. It can be noted how the rate of increase of the Fe concentration is one order of magnitude larger than that of Cr as it is 10 times more present in the EUROFER97. Therefore, the saturation concentration is reached faster, causing the CT to start operating sooner, and a steady state is reached for the Fe concentration after ∼20 hours. On the other hand, the Cr concentration is still increasing at the end of the simulation meaning that the CT is not removing any Cr particle yet.

In Fig. 9 the evolution of the Fe concentration at the CT inlet is shown for different values of the CT efficiency; it is clearly visible that as soon as the saturation is reached, Fe is removed by the CT and its concentration in PbLi quickly reaches a steady state.

Fig. 10 reports the concentration computed at the inlet and outlet of the CT and TBM at the end of the simulation, for both Fe and Cr. Given that the source term adopted for this test case is constant in space, hence its integral gives a constant and exact value, the variation of the ACPs concentration along the TBM at the steady-state is linear and it is not affected by numerical errors due to the spatial discretization. In view of the above, a comparison between the numerical solution and the analytical one is shown in Fig. 10a for Fe. Moreover, from Fig. 10a it can be seen that Fe concentration undergoes a slight increase (6.1×10^{-6} wppm) along the TBM, as a result of a Fe corrosion rate that, in view of a PbLi velocity of ∼0.5 mm/s, can be computed as equal to 0.0046 μm/a. Furthermore, it can be noted that Fe concentration has reached the steady state at this point, as the TBM outlet concentration matches the CT inlet concentration and vice-versa, whereas this is not true for Cr. Indeed, Cr concentration is unchanged between inlet and outlet of the CT (Fig. 10b), as it has not reached the saturation value computed with (17), and its value is slightly lower than that at the outlet of the TBM due to the transit time in the TER, HT and HX, placed between the TBM and the CT in this model (see Fig. 6). For the same reason, the concentration at the inlet of the TBM is lower than that at the outlet of the CT, due to the presence of the PbLi pipes of the circuit, since the transient is not extinguished yet.

In Fig. 11, the comparison between the Fe concentrations at the CT inlet and outlet is shown for different values of the CT efficiency at the steady state. Conversely, the Cr saturation concentration is not reached within the simulated time frame, in view of the (∼4 orders of magnitude) larger value of the saturation concentration itself, as well as of the lower source term (the corrosion rate is computed to be $4.7 \times 10^{-4}\mu$m/a, i.e. about one order of magnitude lower than that of the Fe), so the Cr concentration is still increasing at the end of the transient and the CT is not active yet. For the same reason, changing the cold trap efficiency does not affect the Cr concentration, which after four days is equal to 9.41×10^{-5} wppm regardless of the value of the CT efficiency, as the CT does not remove any Cr impurity. Furthermore, given that the Cr concentration increase is linear in time, it has been evaluated that Cr would reach the saturation in PbLi in ∼18 years, under the current assumption of activation source term S_A and redeposition sink term S_R equal to zero.

Finally, Fig. 12 reports the evolution of the concentration of Fe and Cr in different locations along the TBM channels, for the case of 90 % CT efficiency; also in this case, the same effects mentioned above are visible. Moreover, as a consequence of the small source term for Cr, its concentration is almost uniform along the TBM flow path, as advection is dominating on the source. A small, but non-negligible difference is instead visible for Fe in Fig. 12a when the steady state is reached.

Note that the results presented here are only partial, given the assumptions made on the activation source and redeposition sink, but they show the capability of the model to compute the concentration of ACPs (which could be easily translated into dose rate) anywhere in the loop.

E. RESULTS: TEST CASE II

The models for the IB and OB PbLi loops of the EU DEMO WCLL are run to simulate a transient of 8 hours; as for the test case I, the initial concentration of ACPs in the circuit is set equal to zero and a constant rotational speed for the pump is assumed. In Fig. 13 the evolution of the concentration of Fe and Cr at the CT outlet is shown for both the IB and OB loops. The Fe concentration reached the steady-state in both IB and OB loops within the simulated time frame, since it had already exceeded the saturation limit of $\sim 3.7 \times 10^{-4}$ wppm at 330 °C and, hence, the CT trap started removing Fe particles; on the other hand, Cr concentration is still increasing due to its lower rate of increase and its much higher saturation limit (∼ 1.6 wppm). It can be seen how the increase of the ACPs concentration is faster inside the IB loop with respect to the OB one, as the Fe reaches the steady-state faster and Cr concentration after 8 hours is larger; the reason is that the loop pipes, where PbLi flows with larger velocity with respect to the BB (hence the corrosion rate computed with (13) is larger), are longer in the case of the IB loop.

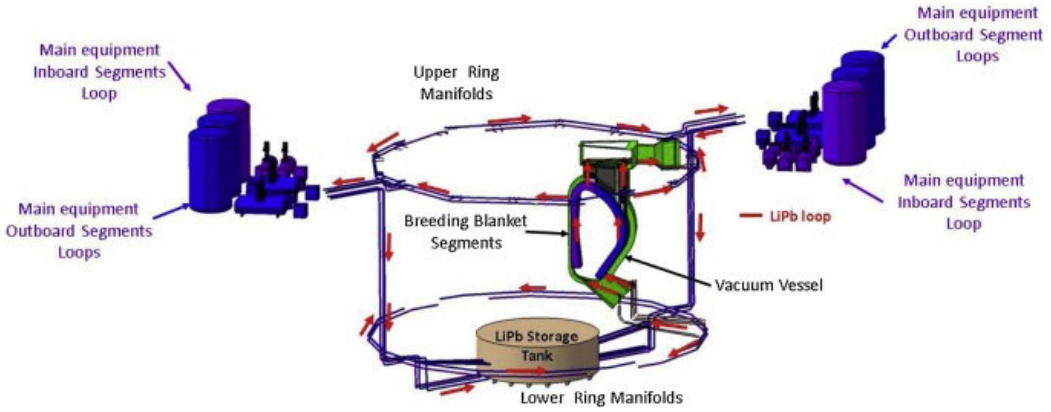

FIGURE 5. Isometric view of the EU DEMO WCLL PbLi loop [26].

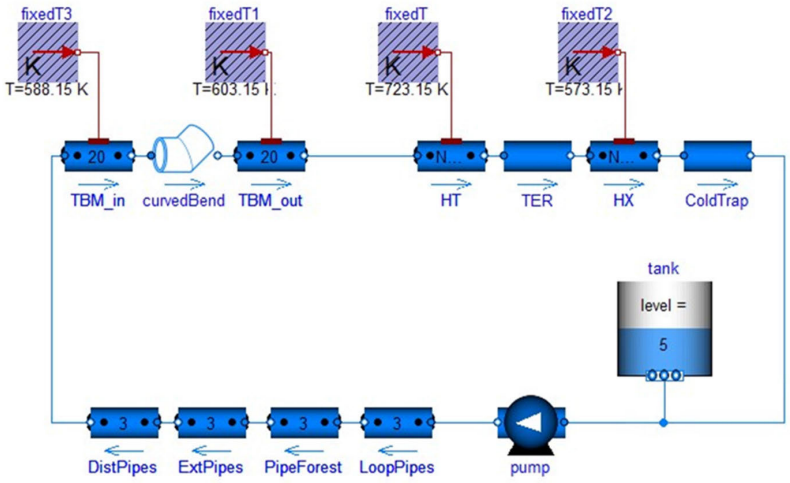

FIGURE 6. Scheme of the circuit model of the WCLL-TBS PbLi loop (test case I).

Moreover, from Fig. 13 it is clearly noticeable a ''staircase'' profile of the curves: this behavior is due to the different rates of corrosion and different PbLi transit times inside the components where corrosion takes place. The intervals during the transient where the concentration profile is almost flat correspond to the transit of PbLi inside the BUs, where the corroded mass of ACPs is low – due to the short path of the working fluid along the component – and the PbLi transit time is long – given the very low flow velocity of ~ 0.3 mm/s. For instance, the PbLi transit time inside the COB BUs is $\sim$ 1.1 h, which is a very large fraction of the overall transit time within the whole circuit ($\sim$ 1.7 h).

Fig. 14 shows the Fe concentration computed after 8 hours inside a IB segment. It is clear that the concentration increase in the segment takes place almost entirely in the inlet and outlet manifolds, while the BUs account for just the 5 % of the total increase. In fact, despite the larger wetted perimeter, the corrosion term computed inside the BUs is limited by the short flow path and the low flow velocity.

Since the model can compute the concentration of ACPs during a transient at any location within the PbLi loops, it is used for the WCLL PbLi loop test case to evaluate the activity (expressed in becquerels per unit volume of PbLi) of the species transported by the working fluid within the different BB segments and loop pipes. In this paper, the results on

TABLE 3. Activity and mass of the activated Fe transported within PbLi in different components of the circuit, for test case II.

COMPONENT	ACP mass [g]	Activity [Bq/m^3]
COB segment	7.65×10^{-2}	2.35648×10^{8} (min) 2.85237×10^{8} (max)
LOB/ROB segment	7.00×10^{-2}	2.35645×10^{8} (min) 2.81606×10^{8} (max)
LIB/RIB segment	3.65×10^{-2}	2.55747×10^{8} (min) 3.08274×10^{8} (max)
OB ex-vessel pipes	1.14×10^{-1}	1.73388×10^{8} (min) 3.31700×10^{8} (max)
IB ex-vessel pipes	1.04×10^{-1}	1.63439×10^{8} (min) 3.81714×10^{8} (max)
OB TER system	-	1.73388×10^{8} (min) 3.31700×10^{8} (max)
IB TER system	-	1.63439×10^{8} (min) 3.81714×10^{8} (max)

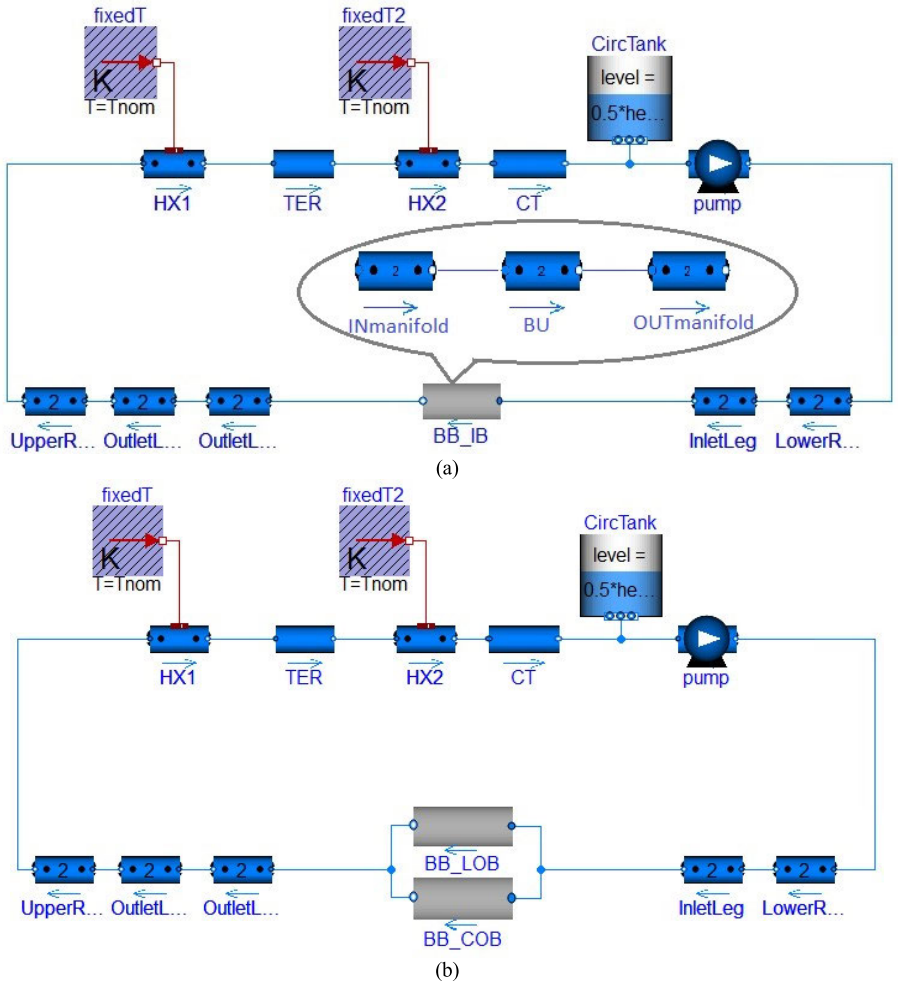

FIGURE 7. Scheme of the circuit models of the EU DEMO-WCLL PbLi loops (test case II): (a) IB loop model with detailed view of the BB object; (b) OB loop model.

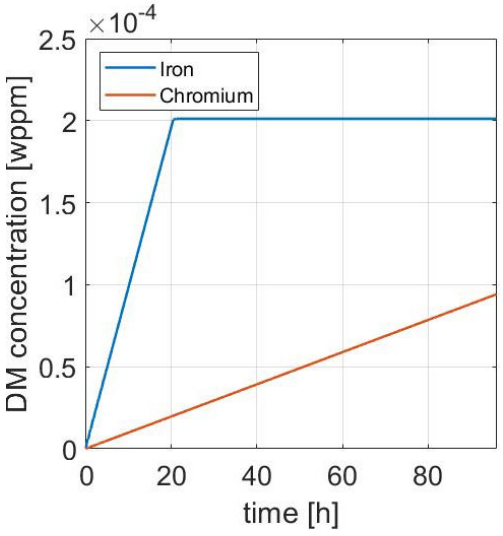

FIGURE 8. Concentration evolution at the outlet of the CT for Fe and Cr.

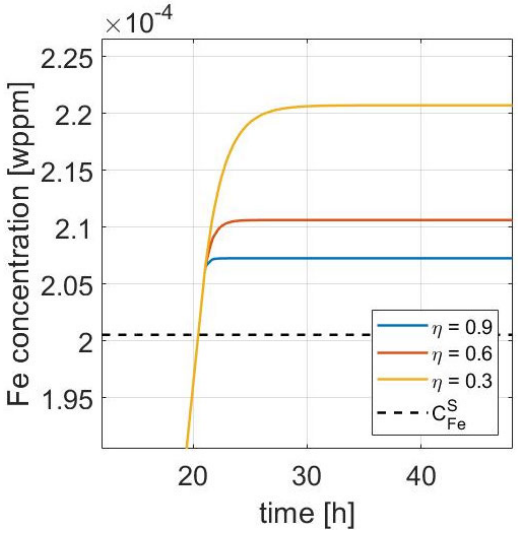

FIGURE 9. Concentration evolution for Fe at the CT inlet for different CT efficiencies η; the black dashed line is the Fe saturation concentration at the prescribed PbLi temperature (575.15 K).

the ACPs inventories are shown only for Fe, given that Cr was still far from reaching the steady-state at the end of the simulations and thus an estimation of its inventories did not seem relevant at this stage. Starting from the overconservative assumption that all the corroded EUROFER97 particles are

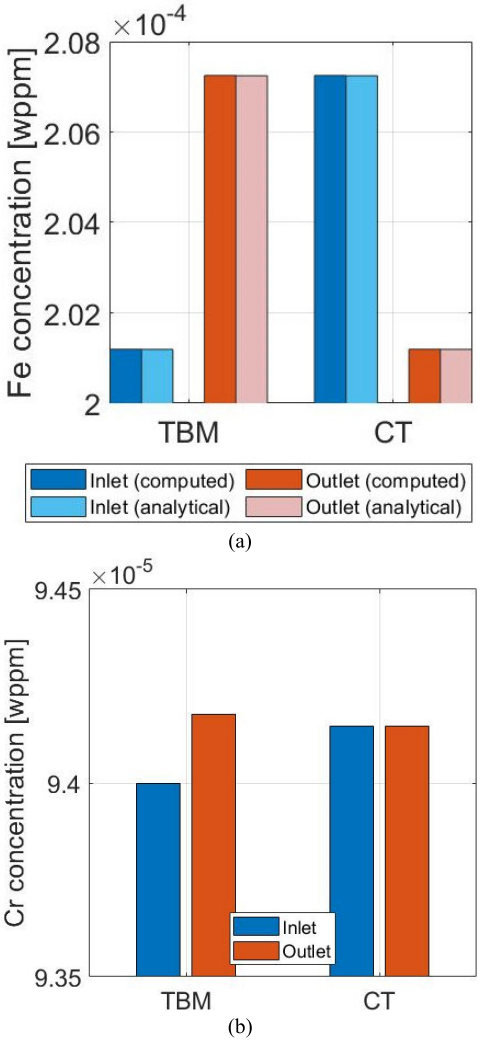

FIGURE 10. Concentration of Fe (a) and Cr (b) at the inlet and outlet of the CT and TBM, after 20 days; for Fe, a comparison between numerical and analytical solution is shown in (a).

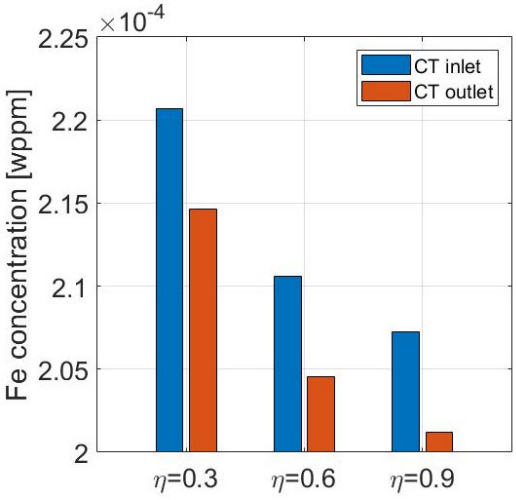

FIGURE 11. Fe concentration at the inlet and outlet of the CT after 20 days, varying its efficiency.

activated and that the activity does not reduce in time due to decay, the concentration computed in different locations of

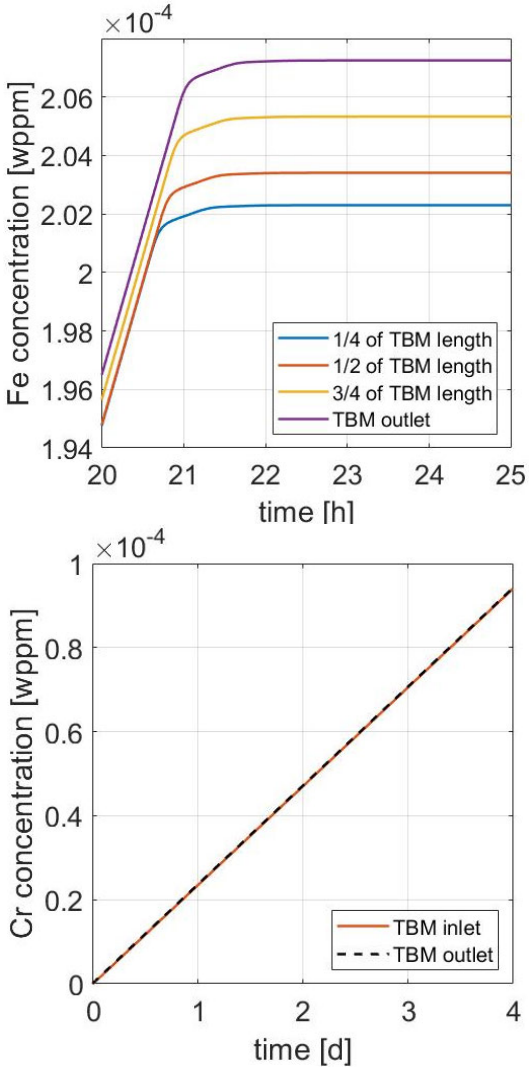

FIGURE 12. Evolution of Fe (a) and Cr (b) concentration, in different CVs along the TBM.

the loop is multiplied by the specific activity of the species involved (i.e. Fe). For the latter, a constant value of 4.32×10^{13}Bq/kg have been assumed in this work.

Table 3 shows the results on the activity per unit volume of PbLi and the masses of ACPs in different components of the IB and OB loops, referred to the steady-state concentration. The masses of Fe in each component is obtained by simply multiplying its concentration in each CV by the mass of fluid contained in a CV, and sum over the total number CVs of the component. Finally, minimum and maximum activity values are provided, corresponding to that computed at the inlet and outlet of each component, respectively. It must be noted that the results reported in Table 3 are affected by the (conservative) assumptions made – for instance, that all the corroded EUROFER97 is activated and that there is no redeposition of ACPs on the wetted surfaces. Nonetheless, it seemed appropriate to report these results to showcase the potential of the model.

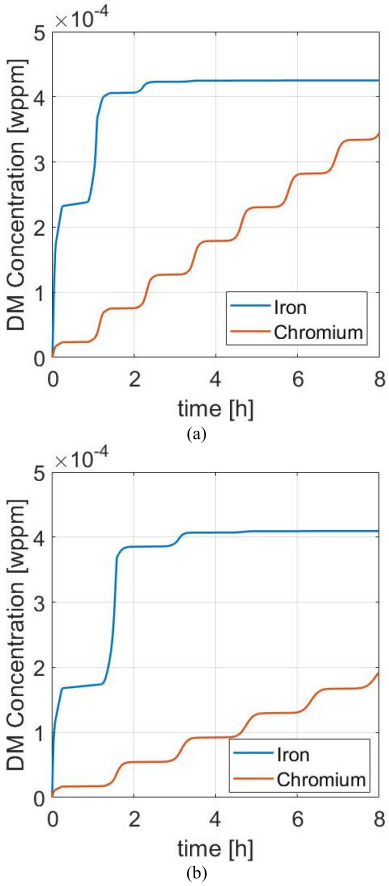

FIGURE 13. Test case II: concentration evolution at the outlet of the CT for Fe and Cr, for the (a) IB loop and (b) OB loop.

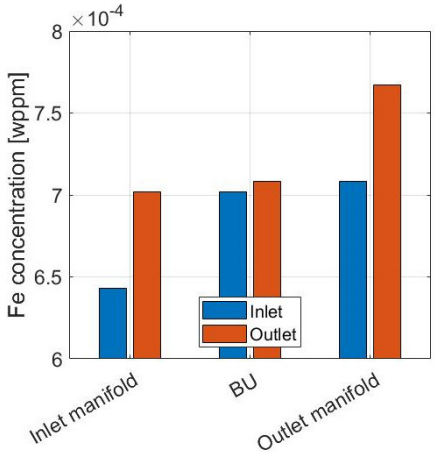

FIGURE 14. Test case II: Fe concentration in an IB segment after 8 hours.

V. CONCLUSION AND PERSPECTIVE

The PbLi loop model available in the GETTHEM system-level code has been extended to include modelling of the ACP generation, transport, and removal.

The model now allows solving the mass conservation for an unlimited number of Dispersed Materials found in trace in the working fluids. Specifically for ACP modelling, source terms (corrosion) are included in the balance, and a 0D model of the cold trap filters has been included. The developed model has been verified with an order-of-accuracy test.

The capability of the model to compute the concentration of a generic DM species in different places of the circuit has been demonstrated. A first test case for the ITER WCLL-TBS loop has been indeed presented, showing that the Fe concentration takes about 20 hours to stabilize, while the Cr (due to its lower corrosion rate and higher saturation concentration for the extraction) does not reach a steady-state distribution in a relevant timespan for the plant. Moreover, a second test case for the EU DEMO WCLL loop has been presented, showing a practical application for this system-level model: the evaluation of the activity and the radioactive inventories of ACPs in different locations of the PbLi loop.

In perspective, the model shall be extended to the transport of other unmixable species, relevant for the EU DEMO WCLL BB as well as the ITER WCLL-TBS, such as helium and tritium; for the latter, a model of the TER is also under development, which might be integrated in the future with a fuel cycle simulator.

ACKNOWLEDGMENT

The authors would like to thank Dr. Alessandro Del Nevo for his appreciated support in the development of the GETTHEM Code.

REFERENCES

[1] A. J. H. Donné, W. Morris, X. Litaudon, C. Hidalgo, D. McDonald, H. Zohm, E. Diegele, A. Möslang, K. Nordlund, G. Federici, P. Sonato, C. Waldon, D. Borba, and P. Helander, "European research roadmap to the realisation of fusion energy," EUROfusion Consortium, Garching, Germany, Tech. Rep., 2018.

[2] A. Froio, C. Bachmann, F. Cismondi, L. Savoldi, and R. Zanino, "Dynamic thermal-hydraulic modelling of the EU DEMO HCPB breeding blanket cooling loops," *Prog. Nucl. Energy*, vol. 93, pp. 116–132, Nov. 2016.

[3] P. Arena, A. D. Nevo, F. Moro, R. Mozzillo, V. Imbriani, F. Giannetti, F. Edemetti, A. Froio, L. Savoldi, A. Tassone, F. R. Urgorri, P. A. Di Maio, I. Catanzaro, and G. Bongiovì, "The DEMO water-cooled lead–lithium breeding blanket: Design status at the end of the pre-conceptual design phase," *Appl. Sci.*, vol. 11, no. 24, 2021, Art. no. 11592.

[4] A. Froio, F. Cismondi, L. Savoldi, and R. Zanino, "Thermal-hydraulic analysis of the EU DEMO helium-cooled pebble bed breeding blanket using the GETTHEM code," *IEEE Trans. Plasma Sci.*, vol. 46, no. 5, pp. 1436–1445, May 2018.

[5] A. Froio, A. D. Nevo, E. Martelli, L. Savoldi, and R. Zanino, "Parametric thermal-hydraulic analysis of the EU DEMO water-cooled lithium-lead first wall using the GETTHEM code," *Fusion Eng. Des.*, vol. 137, pp. 257–267, Dec. 2018.

[6] A. Froio, A. Batti, A. Del Nevo, G. A. Spagnuolo, L. Savoldi, and R. Zanino, "Implementation of a system-level magnetohydrodynamic model in the GETTHEM code for the analysis of the EU DEMO WCLL breeding blanket," Presented at the 24th Top. Meeting Technol. Fusion Energy, Nov. 2020.

[7] G. Mariano, A. Colangeli, D. Flammini, N. Fonnesu, F. Moro, N. Terranova, and R. Villari, "Development of a novel MCNP-OSCAR fusion interface for the 3-D assessment of gamma dose due to the activated corrosion products," *IEEE Trans. Plasma Sci.*, vol. 50, no. 11, pp. 4539–4544, Nov. 2022.

[8] M. D'Onorio, M. Molinari, G. Mariano, and N. Terranova, "RAVEN/OSCAR-fusion coupling for activated corrosion products assessments, sensitivity, and uncertainty quantification," *IEEE Trans. Plasma Sci.*, vol. 50, no. 11, pp. 4527–4532, Nov. 2022.

[9] N. Terranova, L. Di Pace, G. Mariano, S. Breifokaité, F. Broutin, G. Caruso, A. Colangeli, F. Dacquait, M. D. Palma, M. D'Onorio, C. Gasparrini, T. Kaliatka, E. L. Piccolo, M. Molinari, M. T. Porfiri, R. Torella, and R. Villari, "Activated corrosion products assessment and minimization strategies investigated in the EUROfusion safety research program," Presented at the 32nd Symp. Fusion Technol., Dubrovnik, Croatia, 2022.

[10] J. S. Yoon, Y. I. Jung, D. W. Lee, S. K. Kim, H. G. Jin, E. H. Lee, and H. G. Lee, "Corrosion test using ARAA in the experimental loop for a liquid breeder," in *Proc. IEEE 26th Symp. Fusion Eng. (SOFE)*, May 2015, pp. 1–5.
[11] I. Ricapito, A. Aiello, A. Bükki-Deme, J. Galabert, C. Moreno, Y. Poitevin, D. Radloff, A. Rueda, A. Tincani, and M. Utili, "Tritium technologies and transport modelling: Main outcomes from the European TBM project," *Fusion Eng. Des.*, vol. 136, pp. 128–134, Nov. 2018.
[12] S. Meschini, R. Testoni, and M. Zucchetti, "Development of an object-oriented, thermal-hydraulics model for ARC FLiBe loop safety assessment," *Fusion Eng. Des.*, vol. 178, May 2022, Art. no. 113095.
[13] L. Melchiorri, V. Narcisi, F. Giannetti, G. Caruso, and A. Tassone, "Development of a RELAP5/MOD3.3 module for MHD pressure drop analysis in liquid metals loops: Verification and validation," *Energies*, vol. 14, no. 17, p. 5538, Sep. 2021.
[14] F. Casella and A. Leva, "Modelica open library for power plant simulation: Design and experimental validation," in *Proc. 3rd Int. Modelica Conf.*, Linköping, Sweden, Nov. 2003, pp. 1–11.
[15] R. Bonifetto, A. Froio, F. Lisanti, and M. Utili, "Modeling the PbLi flow including tritium transport and permeation with GETTHEM," Presented at the 13th Int. Conf. Tritium Sci. Technol., Bucharest, Romania, Oct. 2022.
[16] F. Casella, M. Otter, K. Proelss, C. Richter, and H. Tummescheit, "The modelica fluid and media library for modeling of incompressible and compressible thermo-fluid pipe networks," in *Proc. 5th Int. Modelica Conf.*, Vienna, Austria, Sep. 2006, pp. 631–640.
[17] R. Franke, F. Casella, M. Sielemann, K. Proelss, and M. Otter, "Standardization of thermo-fluid modeling in modelica. Fluid," in *Proc. Linköping Electron. Conf.*, Como, Italy, Oct. 2009, pp. 1–11.
[18] A. Aiello, "LLE_ACP_TechNote," F4E_D_2HHTUC Version 2.2, Fusion Energy (FE), Barcelona, Spain, Tech. Rep. F4E_D_2HHTUC, 2019.
[19] C. J. Roy, "Review of code and solution verification procedures for computational simulation," *J. Comput. Phys.*, vol. 205, no. 1, pp. 131–156, May 2005.
[20] A. Quarteroni and S. Quarteroni, *Numerical Models for Differential Problems*, vol. 2. Milan, Italy: Springer, 2009.
[21] L. R. Petzold, "Description of DASSL: A differential/algebraic system solver," Sandia Nat. Lab., Livermore, CA, USA, Tech. Rep., SAND-82-8637; CONF-820810-21, 1982.
[22] A. Tincani, R. Forte, C. Ciurluini, F. Giannetti, E. Garrone, M. Bruzzone, K. Abraham, V. A. P. Pierantoni, and A. Tarallo, "WCLL-TBS system design description document—Part on the four main ancillary systems," EFDA_D_2NTPVX Version 1.1, EUROFusion Consortium, Garching, Germany, Tech. Rep. EFDA_D_2NTPVX, 2019.
[23] A. Tincani et al., "Conceptual design of the main ancillary systems of the ITER water cooled lithium lead test blanket system," *Fusion Eng. Des.*, vol. 167, Jun. 2021, Art. no. 112345.
[24] M. Moscardini, F. Galleni, A. Pucciarelli, M. Eboli, A. D. Nevo, S. Paci, and N. Forgione, "Thermo-hydraulic analysis of PbLi ancillary system of WCLL TBM undergoing in-box LOCA," *Fusion Eng. Des.*, vol. 168, Jul. 2021, Art. no. 112614.
[25] J. Aubert, G. Aiello, D. Alonso, T. Batal, R. Boullon, S. Burles, B. Cantone, F. Cismondi, A. D. Nevo, L. Maqueda, A. Morin, E. Rodríguez, F. Rueda, M. Soldaini, and J. Vallory, "Design and preliminary analyses of the new water cooled lithium lead TBM for ITER," *Fusion Eng. Des.*, vol. 160, Nov. 2020, Art. no. 111921.
[26] R. Mozzillo, M. Utili, A. Venturini, A. Tincani, and C. Gliss, "Integration of LiPb loops for WCLL BB of European DEMO," *Fusion Eng. Des.*, vol. 167, Jun. 2021, Art. no. 112379.
[27] E. Martelli, A. Del Nevo, P. Arena, G. Bongiovì, G. Caruso, P. A. Di Maio, M. Eboli, G. Mariano, R. Marinari, F. Moro, R. Mozzillo, F. Giannetti, G. Di Gironimo, A. Tarallo, A. Tassone, and R. Villari, "Advancements in DEMO WCLL breeding blanket design and integration," *Int. J. Energy Res.*, vol. 42, no. 1, pp. 27–52, Jan. 2018.
[28] J. Sannier, M. Broc, T. Flament, and A. Terlain, "Corrosion of austenitic and martensitic stainless steels in flowing $Pb_{17}Li$ alloy," *Fusion Eng. Des.*, vol. 14, nos. 3–4, pp. 299–307, Apr. 1991.
[29] S. Bassini, "Design and qualification of corrosion facility at DCLL relevant condition," EFDA_D_2L3283 Version 1.2, EUROFusion Consortium, Garching, Germany, Tech. Rep. EFDA_D_2L3283, 2015.
[30] T. Zaouter, K. Vulliez, B. Michel, S. Gazzotti, J.-P. Friconneau, and J.-P. Martins, "Assessment of a bolted-flange connection for ITER test blanket module," *Fusion Eng. Des.*, vol. 165, Apr. 2021, Art. no. 112247.

FABRIZIO LISANTI was born in Potenza, Italy, in 1996. He received the B.S. degree in energy engineering and the M.S. degree in energy and nuclear engineering from the Politecnico di Torino, Turin, Italy, in 2018 and 2021, respectively. He is currently pursuing the Ph.D. degree in energy engineering.

From 2021 to 2022, he received a Graduate Research Scholarship in nuclear fusion engineering from the Politecnico di Torino. His research interests include the macro-scale modeling of nuclear fusion devices to perform thermal–hydraulic analyses on the cooling loops for both the cryogenic plant and breeding blanket of tokamaks and the assessment of the generation and transport of tritium and activated corrosion products in the liquid–metal loop of breeding blankets.

PIETRO ARENA was born in Sciacca, Agrigento, Italy, in 1987. He received the master's degree in energy and nuclear engineering and the Ph.D. degree in energy and information technologies from the University of Palermo, in 2012 and 2017, respectively.

From 2012 to 2018, he was a Research Fellow with the University of Palermo, working on the thermo-mechanics of IFMIF-DONES and breeding blankets of fusion reactors, with particular focus on water-cooled lead-lithium (WCLL). From 2018 to 2021, he was awarded a EUROfusion Engineering Grant (EEG) for the support to the design of the IFMIF-DONES lithium loop. Since 2019, he has been a Researcher with the ENEA-Brasimone Research Centre, where he concluded the EEG and continued working on the design of the WCLL breeding blanket. Since 2021, he has been the Lead Engineer of the WCLL breeding blanket, coordinating all the design and research activities on this topic. He has authored and coauthored more than 40 scientific articles in international peer-reviewed journals, such as IEEE TRANSACTIONS ON PLASMA SCIENCE and *Fusion Engineering and Design*.

ROBERTO BONIFETTO (Member, IEEE) received the B.S. and M.S. degrees in energy and nuclear engineering and the Ph.D. degree in energetics from the Politecnico di Torino, Turin, Italy, in 2008, 2010, and 2014, respectively.

He has been an Associate Professor of nuclear engineering with the Energy Department, Politecnico di Torino, since 2021. He has authored or coauthored over 60 articles on international journals, concerning the development, validation, and application of computational tools for the modeling of nuclear fusion and fission devices, the computational fluid dynamics analysis of high-heat fusion components, and the tritium extraction from the EU DEMO breeding blanket. He has been involved, in particular, in the design of the Italian DTT and EU DEMO magnet systems, being the Project Leader of the DTT thermal shield, since 2022.

Prof. Bonifetto is a member of the American Nuclear Society and the Associazione Italiana Nucleare, and regularly serves as a Referee for the IEEE TRANSACTIONS ON APPLIED SUPERCONDUCTIVITY. He received the IEEE Graduate Study Fellowship in applied superconductivity, in 2014, and the European Nuclear Education Network Association Ph.D. Prize, in 2013. He was awarded the EUROfusion Postdoctoral Fellowship and the EUROfusion Engineering Grant, in 2014 and 2016, respectively.

ANTONIO FROIO received the B.Sc. degree in mechanical engineering from Università della Calabria, Rende, Cosenza, Italy, in 2012, the M.Sc. degree in energy and nuclear engineering from the Politecnico di Torino, Turin, Italy, in 2014, the M.Sc. degree in nuclear engineering from the Politecnico di Milano, Milan, Italy, under a double degree program, in 2015, the Alta Scuola Politecnica Diploma degree from the Politecnico di Torino and the Politecnico di Milano, in 2015, and the Ph.D. degree in energetics from the Politecnico di Torino, in 2018.

From 2018 to 2021, he was a Research Fellow with the Energy Department, Politecnico di Torino, where he has been an Assistant Professor, since 2022. He has authored or coauthored more than 30 articles in international journals concerning the development and application of system-level models for tokamak fusion reactors, the CFD analysis of different fusion components, and multi-physics modeling of the breeding blanket. He is involved in the design of the EU DEMO in-vessel components and related auxiliary systems. He is a co-inventor of two patents.

Dr. Froio is a member of the American Nuclear Society and the Associazione Italiana Nucleare. He was awarded the EUROfusion Engineering Grant, in 2018.

FRANCISCO ALBERTO HERNÁNDEZ GONZÁLEZ (Member, IEEE) received the master's degree in industrial engineering from the Universitat Politècnica de Catalunya, in 2006, and the Ph.D. degree in mechanical engineering from Karlsruhe Institute of Technology (KIT), in 2016.

From 2006 to 2009, he was an Automobile Design Development Engineer with EDAG GmbH. In 2009, he was a Product Engineer with RDT Ingenieros, Barcelona, Spain. From 2009 to 2012, he was a Goal Oriented Trainee with EFDA, where he collaborated in the conceptual design of the Breeder Unit for the ITER HCPB TBM concept. From 2013 to 2016, he performed his Ph.D. in mechanical engineering in solid breeder blankets, while he collaborated in the engineering design and procurement of subcomponents of the ITER HCPB TBM for F4E. In 2015, he was appointed as a Lead Engineer for the development of the HCPB concept for the EU DEMO in the frame of the work package breeder blanket with EUROfusion. In 2021, he was the System Design Lead of the Breeding Blanket with the DEMO Central Team, EUROfusion. In 2022, he was the Head of the Design and Analysis of Nuclear Components, Fabrication and Qualification (DAF) Department, Institute of Neutron Physics and Reactor Technology (INR), KIT, as well as the Breeding Blanket Task Force Lead of KIT. Since 2023, he has been the Project Leader of the Work Package Breeding Blanket with EUROfusion. He has authored and coauthored more than 60 scientific articles in international peer-reviewed journals.

Dr. Hernández González is a member of the IEEE Nuclear and Plasma Sciences Society (NPSS), where he has been elected as a member of the NPSS Fusion Technology Standing Committee.

GANDOLFO ALESSANDRO SPAGNUOLO received the master's degree in energy and nuclear engineering from the University of Palermo, in 2014, and the joint Ph.D. degree in mechanical engineering and energy and information technologies from Karlsruhe Institute of Technology (KIT) and the University of Palermo, in 2020.

From 2012 to 2013, he was a Research Fellow with the University of Palermo, working on the thermal–hydraulics of diverters, test blanket modules, and shielding blankets of ITER reactors. In 2013, he was an Intern with ITER, working on the definition of the procedure for the study of the whipping effects of high energy piping. From 2014 to 2015, he worked as a Thermal-Hydraulic and Thermo-Mechanic Analyst as well as a System Engineer with Kraftanlagen Heidelberg GmbH. From 2015 to 2018, he was awarded the EUROfusion Engineering Grant (EEG) for the support to the design of the DEMO breeding blanket concepts. Since 2015, he has been a Researcher with KIT, where he concluded the EEG and the Ph.D. while working with the Management and support Design Integration Team (MDIT) on the project control, system engineering, and requirements definition and management. Since 2020, he has been seconded with EUROfusion, where he covered several roles such as Breeding Blanket Design Integration Engineer, Senior Coordinator with TBM research and development activities, and Area Manager for the integration of the in-vessel components. He has authored and coauthored more than 30 scientific articles in international peer-reviewed journals.

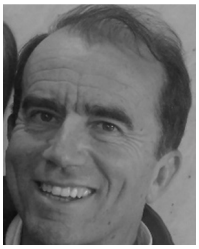

ROBERTO ZANINO (Senior Member, IEEE) received the M.Sc. degree in nuclear engineering and the Ph.D. degree in energetics from the Politecnico di Torino, Turin, Italy.

He has been a Professor of nuclear engineering with the Energy Department, Politecnico di Torino, since 2000. He has authored or coauthored over 200 articles that appeared in international journals devoted to the computational modeling in the fields of relevance for nuclear fusion (superconducting magnets and cryogenics, plasma–wall interactions, and high heat flux components), nuclear fission (Gen-IV lead-cooled fast reactors), and concentrated solar power (central tower system receivers).

Prof. Zanino is a member of the American Nuclear Society and regularly serves as a Referee for IEEE TRANSACTIONS ON APPLIED SUPERCONDUCTIVITY.

Open Access funding provided by 'Politecnico di Torino' within the CRUI CARE Agreement